Nucleation of self-growth dislocations on growth front during the solidification process of silicon

View Online   Export Citation   CrossMark

Naigen Zhou,[1] Xiaoxiao Sui,[1] Xiajie He,[1,2] Shaowen Huang,[1,a] and Lang Zhou[1]

AFFILIATIONS

[1]School of Materials Science and Engineering/Institute of Photovoltaics, Nanchang University, Nanchang 330031, China
[2]The Attached Middle School to Jiangxi Normal University, Nanchang 330031, China

[a]Author to whom correspondence should be addressed: shaowen_huang@163.com

ABSTRACT

Molecular dynamics simulation of the nucleation of dislocations in the solidification of silicon has been carried out. The self-growth dislocations could be generated on growth front of grains with the reduction of local energy during homogenous nucleation and growth of silicon. The nucleation mechanism of the self-growth dislocation has been discussed; the essence of it is the mismatch of two atomic islands with different twin stacking sequences in the rough interface. Temperature could affect the interface morphology and then the generation of self-growth dislocation. In addition, some dislocations move along twin boundaries in the grain and even are absorbed by grain boundaries in the course of crystal growth.

I. INTRODUCTION

Because dislocation adsorbs the surrounding impurity atoms and becomes the recombination center of minority carriers,[1–4] it has turned out to be the most critical defect affecting photoelectric conversion efficiency of a multicrystalline silicon (mc-Si) solar cell. Lowering the dislocation density in mc-Si is one of the goals of sustained effort in the photovoltaic field. Among a multitude of related technologies, it is worth mentioning the high performance mc-Si (HP mc-Si) technology.[5,6] It reduces the dislocation density considerably through leading into numerous grain boundaries, which can absorb dislocations or prevent the propagation and extension of dislocations.[7,8] Therefore, HP mc-Si possesses better performance and has become the mainstream in the photovoltaic market. However, related technical improvements are continuing because there are still dislocations in HP mc-Si.

Researchers are trying to improve the growth conditions of the Si ingot so as to reduce the dislocation density in industry. For example, the more uniform the temperature distribution, the better the seeding control growth[6,8,9] and nucleation agent-assisted growth[8,10] in HP mc-Si technology. The current dislocation density in HP mc-Si is much lower compared to that in common mc-Si. Whether the continual optimization for external growth conditions can thoroughly eliminate dislocations or not becomes a puzzling question. Consequently, it is necessary to deeply understand the

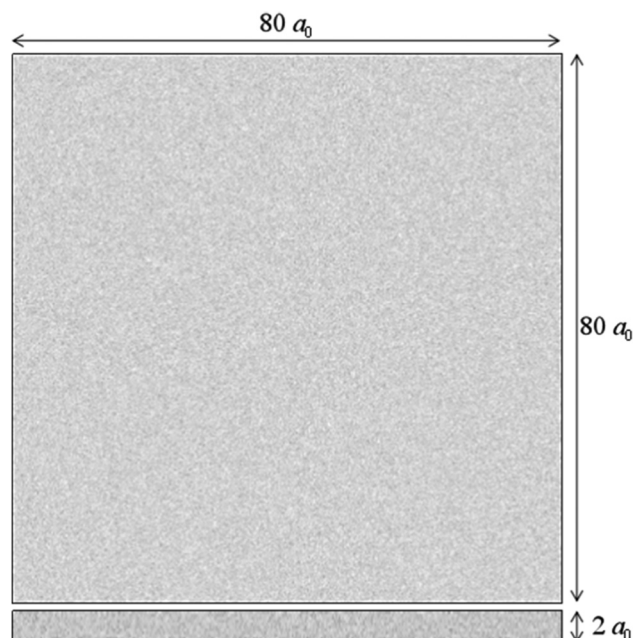nucleation mechanism and microscopic behaviors of dislocations for answering this question.

It is commonly believed that dislocations mainly generate near the liquid–solid interface during the Si crystal growth, and most of them originated from grain boundaries, especially the small angle grain boundaries.[11–15] The migration of dislocations depends on the crystal orientation that determines the slip system.[16–18] Since it is difficult to observe the whole process of dislocation generation and migration experimentally, a lot of molecular dynamics (MD) simulations[19] are performed to study various behaviors of dislocations by tracking the trajectory of every atom. For instance, Justo[20,21] investigated the interaction of intrinsic point defects with 30° glide partial dislocation, and the glide subsets more likely became the core of this dislocation in the competition between the two alternative positions (shuffle and glide {111} plane subsets). Li et al.[22] and Jing et al.[23] studied the influence of temperature on movement velocity of dislocation, and the essence of which was the stress effect. Researchers[24–26] also found that dislocations generated in crystal growth along the specific directions (⟨111⟩ and ⟨112⟩), and they could affect the morphology of the liquid–solid interface and the crystal growth rate. In this work, we construct an ideal growth condition without any external interference to investigate whether dislocation can generate during the native growth process, the nucleation mechanism, and the movement of dislocation if it can.

We hope to provide a reference for the dislocation theory and the production of high quality mc-Si.

II. METHODS

The large-scale atomic/molecular massively parallel simulation (LAMMPS)[27] is employed with the Stillinger–Weber (SW)[28] potential that describes the interaction of Si atoms. The constant pressure–temperature ensemble (NPT) and periodic boundary conditions along all directions are adopted. The Nose–Hoover thermostat and barostat are applied to control the temperature and pressure of the system, respectively. The time step of the simulations is 0.001 ps. In order to create an ideal growth environment without any external disturbance, the pure Si melt is built for homogeneous nucleation and crystal growth. Figure 1 shows the initial atom configuration of the simulation cell by heating a Si crystal with the size of $80a_0 \times 80a_0 \times 2a_0$ (a_0 is the lattice constant, about 102 400 atoms) at $1.48T_m$ (T_m is the melt point of silicon) for 50 ps. The Si melt is subsequently cooled at a cooling rate of 10^{13} K/s down to supercool melt state, and then run for 2000 ps at $0.74T_m$.

To monitor microstructure changes in the solidification process, the dislocation extraction algorithm (DXA) analysis of the open visualization tool (OVITO) is used to distinguish different atom structures: face-centered-cubic (FCC), hexagonal close-packed (HCP).[29,30] The FCC and HCP structures are the characteristics of crystalline phase, and the latter always exists in the stacking faults or twin boundaries. DXA analysis has been widely used in the studies about crystal defects.[25,31] Furthermore, a professional software of image analysis, Image Pro Plus, is applied to measure the grain size. The diameter of grains is measured every 2° intervals passing through its centroid and shows the final calculated average value.

III. RESULTS AND DISCUSSION

A. Solidification processes of Si melt

Figure 2 shows the visualization processes of the homogeneous nucleation and subsequent crystal growth during 2000 ps simulation at $0.74T_m$. The white atoms represent disordered atoms, i.e., melt atoms or grain-boundary atoms. The blue and orange atoms represent the FCC and HCP atoms, respectively. The snapshot of 10 ps cannot find any nuclei, which is similar to that of the initial Si melt in Fig. 1. At 150 ps, several small nuclei nucleated, then more nuclei
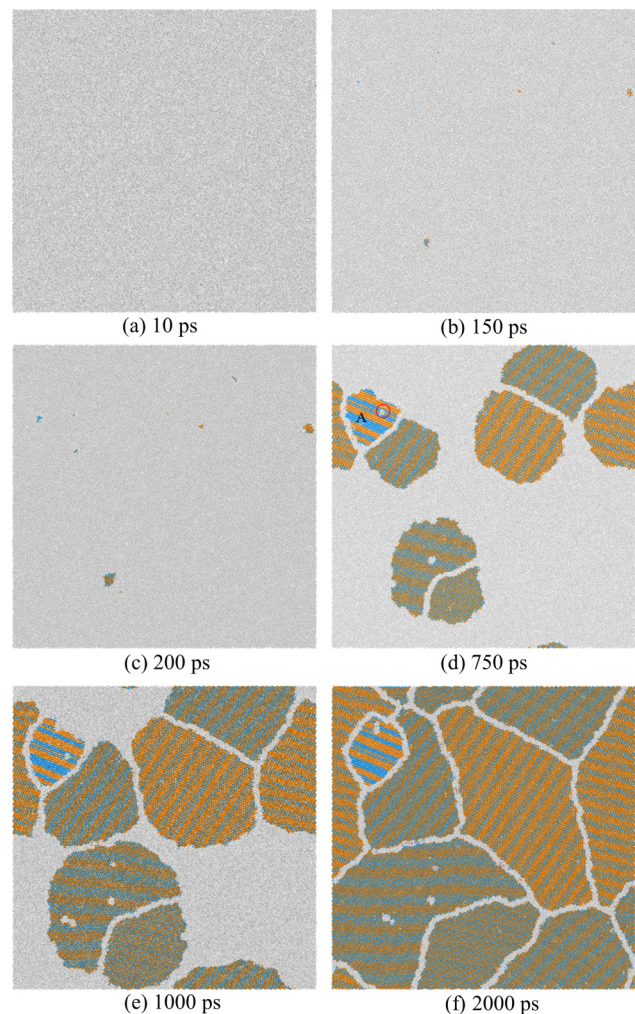
FIG. 1. The molecular dynamics model of homogeneous nucleation and growth from Si melt (size: $80a_0 \times 80a_0 \times 2a_0$, a_0 is the lattice constant of Si crystal).

(a) 10 ps   (b) 150 ps

(c) 200 ps   (d) 750 ps

(e) 1000 ps   (f) 2000 ps

FIG. 2. The XY projection snapshots of solidification process from the Si melt at $0.74T_m$. The white atoms represent melt atoms or grain-boundary atoms. The blue atoms and orange atoms represent the FCC atoms and HCP atoms, respectively.

appeared at 200 ps. It follows that the nucleation of the Si melt at $0.74T_m$ can be considered as the sporadic nucleation model,[32–34] in which the grains grow with further nucleation. At 200 ps, the nucleation stage finished and then grains grew. In the initial growth stage, the grains grew along all directions without limitation. At 750 ps, the crystalline region is about 30% and the grain growth directions are restrained by the surrounding grains. At 1000 ps, the crystalline region is up to 56% and the growth of each grain is affected by two surrounding grains at least. Subsequently, the system is filled with grains with different orientations and shapes at 2000 ps. It can be seen that the grains contain a large number of twin boundaries, which is consistent with the reports in Refs. 34 and 35. The white region in the internal of Grain A is identified preliminarily as a dislocation structure by DXA analysis, and we will further confirm it in Sec. III B. This dislocation is called as a self-growth dislocation because it is generated during the crystal growth process without any external interference, such as impurity, external stress, and internal defect of grains.

B. Structural analysis

Figure 3(a) shows the rotated snapshot in which the {110} plane of Grain A at 750 ps is parallel to the paper. DXA analysis has identified that the disordered region is a dislocation structure with the Burgers vector of $1/6 \langle 112 \rangle$. In order to confirm it, the Burgers circuit measure[36] is applied artificially. Figure 3(b) is the partially enlarged view of the red rectangle region in Fig. 3(a), and the red circuit with arrows is the Burgers circuit that is marked artificially. Supposing that the paper is parallel to the (110) plane, and the close-packed plane $(1\bar{1}1)$ is perpendicular to the paper. $\langle 111 \rangle$ and $\langle 112 \rangle$ directions are also noted in the picture. The Burgers vector b confirmed through the Burgers circuit $MNOPQ$ is $1/6 \langle 112 \rangle$ as well, which is in accordance with the result of DXA analysis. The dislocation line is perpendicular to the Burgers vector b, which indicates that it is an edge dislocation. It is thus confirmed that the white disordered region in the interior of Grain A represents the core of an edge dislocation.

The dislocation produces the strain field in the surrounding medium, which are accompanied by the elastic strain energy. To some extent, the energy needed for the dislocation nucleation could be reflected by the elastic strain energy. The energy increases with

the length of dislocation line, so the energy of dislocation is defined by the unit length of dislocation, which can be expressed as[37]

$$w = \frac{\mu b^2}{4\pi(1-\nu)} \ln \frac{R}{r_0}, \qquad (1)$$

where μ is the shear modules of the material; ν is the Poisson ratio; b is the modulus of the Burgers vector of the dislocation and is $1/6 \langle 112 \rangle$; R is the biggest radius of the dislocation strain field; and r_0 is the initial radius of the dislocation strain field. In the Si crystal, the shear modules $\mu = 57.40$ GPa;[25] the Poisson ratio $\nu = 0.252$;[38] r_0 is the radius of Si atom, about 1.17×10^{-10} m.[25] The value of R is usually used 10^{-6} m,[25] but it is much greater than the size of grains with dislocation. Therefore, the grain size should be used as R to calculate the strain energy. For example, the approximate radius of Grain A at 750 ps is used for the value of R, about 3.37×10^{-9} m. Thus, the energy of this edge dislocation is about 0.63 eV/Å. However, the finite simulation system results in small grain with a shorter radius of the dislocation strain field than that in the real crystal. The smaller elastic strain energy of dislocation represents the less energy needed to nucleate. Furthermore, from Eq. (1), the strain energy w is logarithmically proportional to the radius of its strain field R, and is in proportion to b^2. The dislocation with smallest b ought to be the most stable one in the crystal from the point of view of energy, which can be comprehended as that the slipping orientation of dislocation always follows the atom close-packed orientation.

C. Nucleation process of dislocation

The dislocation as shown in Fig. 3 is generated on growth front of grains without any external interference during crystal growth. The nucleation process of the dislocation should be interesting and different from that of the usual dislocation. In this section, the structural and energy analyses of the dislocation nucleation are briefly outlined. Figure 4 shows the structural analysis of the dislocation nucleation process in Grain A. The blue and orange atoms are FCC and HCP atoms, respectively. It can be seen that all the twin boundaries are parallel to each other and to the growth interface of {111} plane. Along the $\langle 111 \rangle$ growth direction, the liquid–solid interface of the grain shows the island shape at 550 ps. This interface shape results from the thermal fluctuation that is induced by the released latent heat of crystallization from the liquid–solid interface. However, once the growth of these island-shaped interfaces are nonsynchronous, the disordered structure will be easily formed at the junction of these islands. In Fig. 4(b), the dashed line L_1 is the bilayer atom structure whose left region is HCP stacking sequence and the right region is FCC stacking sequence. The encounter of the HCP and FCC stacking sequences can trigger the initial nucleation of dislocation.[24] At 650 ps, the dislocation is nucleated at the junction of islands between L_1 and L_2, the latter is a new bilayer atom structure with FCC stacking sequence. At 660 ps, some HCP atoms gradually arrange near L_2 during the crystal growth, and a new twin boundary is formed at 720 ps. The green line in Fig. 4(f) is the dislocation line with the Burgers vector of $1/6 \langle 112 \rangle$, which is also confirmed by Burgers circuit artificially. It can be seen that the dislocation is continual and run through the grain to terminate on the crystal surface.
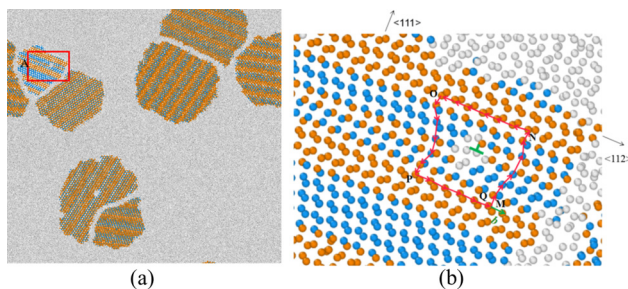
FIG. 3. The rotated snapshot (a) and the enlarged view (b) of the red rectangle at 750 ps.
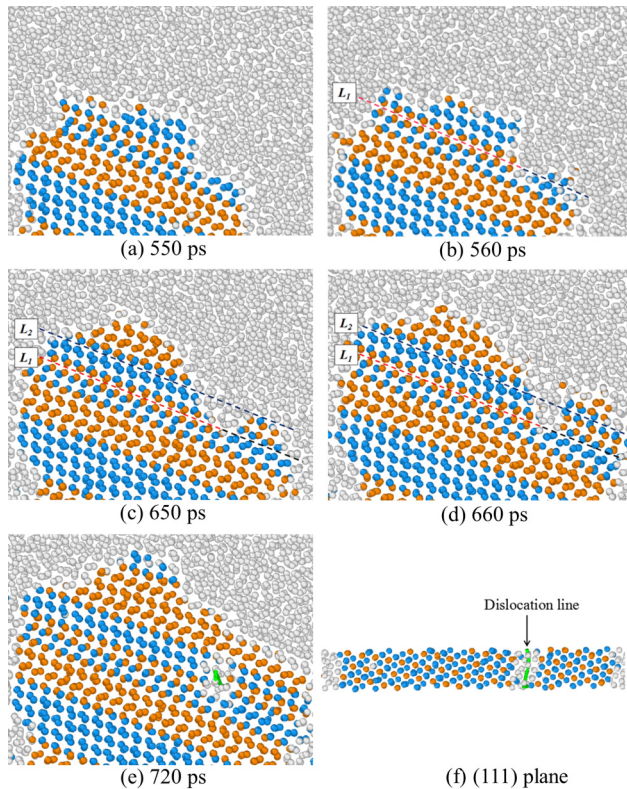
FIG. 4. The nucleation processes of the dislocation in the interior of specific grain.

FIG. 5. The potential energy varying with distance at different times.

The nucleation of dislocation is generally accompanied with the variation of potential energy. The partial region between L_1 and L_2 is chosen to study the changes of potential energy, and the average potential energy of atoms per 0.5 nm region from left to right is calculated. Figure 5 shows the potential energy varying with distance at different times, and the snapshot at the bottom of the figure is the atom configuration at 720 ps. It can be seen that the energy of crystal regions fluctuates between −4.17 eV and −4.10 eV, and the energy of melt/disordered regions is greater than −3.97 eV. After calculation, the average energy of melt/disordered atoms is higher about 0.26 eV than that of the crystal atoms. The changing trends of curves are basically consistent at 550 ps and 560 ps. The left regions have both crystal atoms and melt atoms; thus, their energies are higher than that of the middle crystal regions. The right of the curve of 550 ps shows an upward trend, as these regions are melt atoms with higher energy. At 560 ps, several crystal atoms have appeared at the right regions; thus, the energy slightly decreases. The crystal atoms gradually accumulate and the melt are transformed into crystal during solidification. Consequently, the energies of left and right regions drop as shown in the curve of 650 ps. After that, the trend of the curves has not changed much, which also represents that the dislocation has been generated. The position of highest peak is just the dislocation core as shown in the bottom atom configuration, and the appearance of this peak is in agreement with our structure analysis
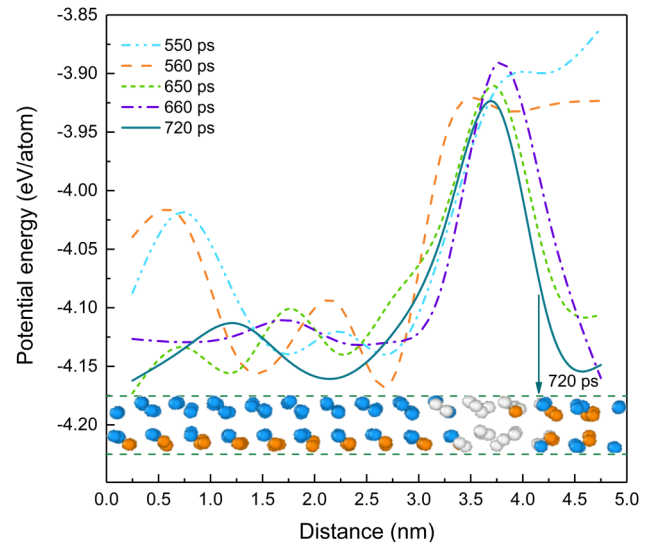
of dislocation nucleation. Moreover, the curves slightly change varying with time on account of the constant fluctuation of the atom energy in the course of crystal growth.

Several kinds of dislocations exist in the Si crystal, such as perfect dislocation, partial dislocation, and unconventional dislocation. In general, the generation of perfect dislocation and partial dislocation is always without and with twin boundary in simulations, respectively. It is obvious that the nucleation of dislocation with the Burgers vector of $1/6 \langle 112 \rangle$ observed in our simulations is accompanied by twin boundary. The fundamental cause of the self-growth dislocation generation is the formation of atomic level island-shaped rough interface on growth front of grains with twin boundaries that are easily generated in grains on account of the low formation energy.[39–44] Once two islands with different stacking sequences of twins merged, the dislocations will be easily nucleated. In addition, the more detailed relationship between dislocation nucleation and twins is required for further study.

Any external growth conditions that can affect the island-shaped interface will influence the formation of self-growth dislocations. It is well known that temperature is one of the key factors that determine the morphology of liquid–solid interface and crystal growth rate. The statistics in Table I shows the number of self-growth dislocations at different temperatures of 3000 ps. It is regrettable that the crystallization at higher temperatures did not simulate due to a long nucleation time and a large system over the limitation of our simulations. It has been proved that the crystallization kinetic process is fast under small degree of undercooling,[45] and the kinetic process is rapid in simulations as well. From the standpoint of kinetic, the simulation and experiment results could be compared to some extent, although the temperatures are different.

The results in Table I may illustrate the effect of temperature on the nucleation of self-growth dislocations. The growth rate and the grain size varying with temperatures have been discussed in our

TABLE I. The number of self-growth dislocations at different temperatures of 3000 ps.

Temperature	$0.77 T_m$	$0.74 T_m$	$0.71 T_m$	$0.68 T_m$	$0.65 T_m$
Dislocation number	3	2	2	0	0

previous work,[34] in which the grain growth rate increases and the grain size decreases as temperatures decrease from $0.77T_m$ to $0.65T_m$. The rapid grain growth rate and small grain size will go against the formation of island-shaped interface. Thus, as the statistics in Table I show, the number of self-growth dislocations decreases with decreasing temperatures. However, the result needs further textual research studies because of the small number of samples and the lack of repeated simulations for the long calculation time.

D. Migration process of dislocation

After the nucleation of self-growth dislocations, some of them will migrate and even be absorbed by grain boundaries, while most of them retain in grains during the crystal growth process. Figure 6 shows a migration process of an edge dislocation. The region in the red circle is the dislocation core, and the green line is the dislocation line with the Burger vector of $1/6\langle 112\rangle$. It will cause the new arrangement of atoms in the movement of dislocation due to the great distortion in the center of dislocation, which will result in a strain field. Thus, the dislocation slipping must overcome the energy barrier of the crystal lattice, which is also called the Peierls–Nabarro stress whose expression is given as follows:[46,47]

$$\tau_{p-n} = \frac{2\mu}{1-\nu}exp\left(-\frac{2\pi}{1-\nu}\cdot\frac{a}{b}\right),\qquad(2)$$
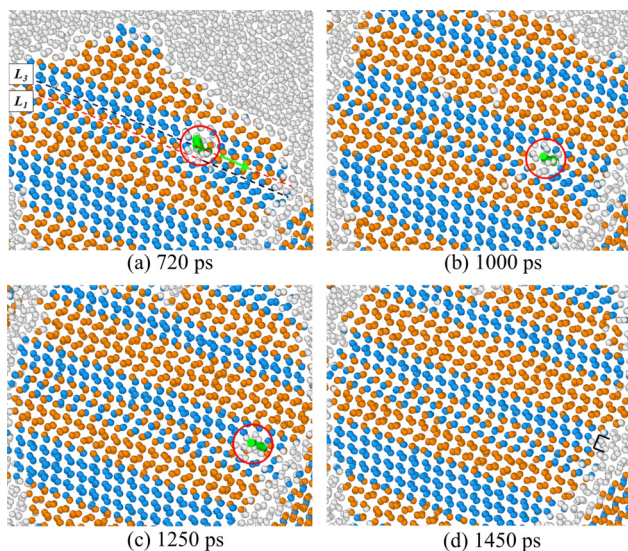
FIG. 6. The migration process of the dislocation in the interior of specific grain.

where μ is the shear modules of the material; ν the Poisson ratio; a is the interplanar spacing of the slipping plane; and b is the modulus of the Burgers vector of the dislocation. By calculation, the critical shear stress τ_{p-n} required to move a single dislocation to overcome lattice resistance is about $7\times10^{-3}\mu$m, which is in complete accord with the statement of Gerold[48] that the τ_{p-n} of covalent crystal is about $\sim10^{-3}\mu$m. a of the atomic close-packed plane {111} is the biggest and the $\langle 110\rangle$ orientation is the atomic close-packed orientation. The dislocation is inclined to generate and migrate along the close-packed {111} plane[49] owing to the smallest τ_{p-n}. Theoretically, the slip system should be {111}$\langle 110\rangle$, but this dislocation slips on the {111}$\langle 112\rangle$ slip system. The main reason is the nanoscale grains and twin boundaries, as reported in Ref. 50. In addition, this dislocation slipping mode belongs to the soft mode,[50–53] in which the slipping plane as well as the slipping direction is parallel to the twin boundary as schematically shown in Fig. 6. The dislocation slips along the direction of the green arrow on the {111}$\langle 112\rangle$ slip system, and it costs about 730 ps to slip from the position of Fig. 6(a) to disappear at the grain boundary as shown in Fig. 6(d). The new bilayer atom structure is indicated as L_3 whose left region is the FCC stacking sequence and right region is the HCP stacking sequence as shown in Fig. 6(a). The atoms stacking sequences of L_1 and L_3 where the dislocation has passed through are changed from FCC stacking and HCP stacking to HCP stacking and FCC stacking, respectively. In other words, the slipping of the dislocation gives rise to a migration of the twin boundaries, namely, leading to induced twinning or detwinning.[50,53] At 1450 ps, the dislocation is completely absorbed by the grain boundary, and a slip step whose width is equal to the Burgers vector is formed as shown by the black sign.

IV. CONCLUSION

The nucleation of dislocation on growth front in the solidification of Si melt was investigated by MD simulations. The twin boundaries and dislocations could be generated in the interior of grains without any external interference. Due to the atomic island-shaped rough interface and the low twin formation energy, self-growth dislocation was easy to be generated at the junction of two islands that accompanied different twin stacking sequences. The generation of self-growth dislocation was also accompanied with the variation of local potential energy, and the energy of dislocation center region was much higher than that of the crystal region. Temperature could affect the interface morphology and then influence the generation of self-growth dislocations. Some of dislocations could move and be absorbed by grain boundaries during the process of solidification.

The number of dislocation nucleation and subsequent multiplication determine the dislocation density in mc-Si. Improving growth conditions, such as temperature distribution, seed species, and grain size of seeds, has largely reduced the dislocation density of mc-Si, but it could not completely eliminate dislocations. The growth process of nucleus in our simulations is similar to that of seeds in high performance mc-Si. It follows that it is quite difficult to prevent the nucleation of dislocations completely in this growth pattern because dislocations could nucleate on growth front without any external interference during the crystal growth. The effective way to reduce dislocation density is to prevent the

dislocation propagations or multiplications, as high performance mc-Si inhibit dislocation multiplications by numerous grain boundaries. It is hoped that the nucleation mechanism and migration behavior of the self-growth dislocation, which is studied in this work, could provide some inspiration on preventing dislocation multiplications and reducing dislocation density.

ACKNOWLEDGMENTS

REFERENCES

[1]K. Kutsukake, T. Abe, N. Usami, K. Fujiwara, I. Yonenaga, K. Morishita, and K. Nakajima, J. Appl. Phys. **110**, 083530 (2011).

[2]H. J. Su, J. Zhang, L. Liu, and H. Z. Fu, Trans. Nonferrous Metal. Soc. **22**, 2548 (2012).

[3]H. Sugimoto, M. Tajima, T. Eguchi, I. Yamaga, and T. Saitoh, Mater. Sci. Semicond. Process. **9**, 102 (2006).

[4]H. Sugimoto, K. Araki, M. Tajima, T. Eguchi, I. Yamaga, M. Dhamrin, K. Kamisako, and T. Saitoh, J. Appl. Phys. **102**, 054506 (2007).

[5]I. Buchovska, O. Liaskovskiy, T. Vlasenko, S. Beringov, and F. M. Kiessling, Sol. Energy Mater. Sol. Cells **159**, 128 (2017).

[6]Y. M. Yang, A. Yu, B. Hsu, W. C. Hsu, A. Yang, and C. W. Lan, Prog. Photovolt. Res. Appl. **23**, 340 (2013).

[7]G. Stokkan, Y. Hu, Ø Mjøs, and M. Juel, Sol. Energy Mater. Sol. Cells **130**, 679 (2014).

[8]C. W. Lan, Y. M. Yang, A. Yu, Y. C. Wu, B. Hsu, W. C. Hsu, and A. Yang, Solid State Phenom. **242**, 21 (2015).

[9]D. D. Zhu, L. Ming, M. L. Huang, Z. Y. Zhang, and X. M. Huang, J. Cryst. Growth **386**, 52 (2014).

[10]Y. T. Wong, C. T. Hsieh, A. Lan, C. Hsu, and C. W. Lan, J. Cryst. Growth **404**, 59 (2014).

[11]B. Ryningen, G. Stokkan, M. Kivambe, T. Ervik, and O. Lohne, Acta. Mater. **59**, 7703 (2011).

[12]D. Oriwol, E. R. Carl, A. N. Danilewsky, L. Sylla, W. Seifert, M. Kittler, and H. S. Leipner, Acta. Mater. **61**, 6903 (2013).

[13]T. Ervik, M. Kivambe, G. Stokkan, B. Ryningen, and O. Lohne, Acta. Mater. **60**, 6762 (2012).

[14]D. Oriwol, M. Hollatz, and M. Reinecke, Energy Procedia **27**, 66 (2012).

[15]Y. Hayama, T. Matsumoto, T. Muramatsu, K. Kutsukake, H. Kudo, and N. Usami, Sol. Energy Mater. Sol. Cells **189**, 239 (2019).

[16]K. Jiptner, Y. Miyamura, B. Gao, H. Harada, K. Kakimoto, and T. Sekiguchi, Solid State Phenom. **242**, 15 (2015).

[17]K. Jiptner, Y. Miyamura, H. Harada, B. Gao, K. Kakimoto, and T. Sekiguchi, Prog. Photovolt. Res. Appl. **24**, 1513 (2016).

[18]D. Oriwol, M. Trempa, L. Sylla, and H. S. Leipner, J. Cryst. Growth **463**, 1 (2017).

[19]M. P. Allen and D. J. Tildesley, Computer Simulation of Liquids (Oxford University Press, Oxford, 1987).

[20]J. F. Justo, K. M. De, W. Cai, and V. V. Bulatov, Phys. Rev. Lett. **84**, 2172 (2000).

[21]J. F. Justo, M. D. Koning, C. Wei, and V. V. Bulatov, Mater. Sci. Eng. **309–310**, 129 (2001).

[22]C. X. Li, Q. Y. Meng, G. Li, and L. J. Yang, Superlattices Microstruct. **40**, 113 (2006).

[23]Y. H. Jing, Q. Y. Meng, and W. Zhao, Phys. B Condens. Matter **404**, 2138 (2009).

[24]N. G. Zhou, X. Y. Wu, X. Q. Wei, L. Zhou, Y. P. Wan, and D. L. Hu, J. Cryst. Growth **443**, 15 (2016).

[25]C. Zhang, Y. R. Luo, K. Li, N. G. Zhou, and L. Zhou, Appl. Phys. A. **122**, 954 (2016).

[26]C. Zhang, B. Liu, K. Li, N. G. Zhou, and L. Zhou, "The effects of dislocations on the crystal growth rate of Silicon-A molecular dynamics study," in International Conference on Advanced Material Engineering (Atlantis Press, 2016).

[27]S. Plimpton, J. Comput. Phys. **117**, 1 (1995).

[28]F. H. Stillinger and T. A. Weber, Phys. Rev. B. **31**, 5262 (1985).

[29]A. Stukowski, Modell. Simul. Mater. Sci. Eng. **18**, 015012 (2009).

[30]A. Stukowski, Modell. Simul. Mater. Sci. Eng. **20**, 45021 (2012).

[31]J. Pohl, M. Müller, A. Seidl, and K. Albe, J. Cryst. Growth **312**, 1411 (2010).

[32]C. C. Ibeh, Thermoplastic Materials Properties, Manufacturing Methods, and Applications (CRC Press, Boca Raton, 2011).

[33]Y. Shibuta, S. Sakane, E. Miyoshi, S. Okita, T. Takaki, and M. Ohno, Nat. Commun. **8**, 10 (2017).

[34]X. X. Sui, Y. J. Cheng, N. G. Zhou, B. B. Tang, and L. Zhou, CrystEngComm **20**, 3569 (2018).

[35]T. F. Li, H. C. Huang, H. W. Tsai, A. Lan, C. Chuck, and C. W. Lan, J. Cryst. Growth **340**, 202 (2012).

[36]F. C. Frank, The London, Edinburgh, and Dublin Philos. Mag. J. Sci. **42**, 809 (1951).

[37]P. H. John and J. Lothe, Theory of Dislocations, 2nd ed. (Wiley, New York, 1982).

[38]C. X. Li, Q. Y. Meng, and K. Y. Zhong, Int. J. Mod. Phys. B **23**, 2365 (2009).

[39]M. Murayama and T. Nakayama, Phys. Rev. B. **49**, 4710 (1994).

[40]B. Delley, J. Chem. Phys. **113**, 7756 (2000).

[41]J. E. Butler and I. Oleynik, Philos. Trans. **366**, 295 (2008).

[42]B. M. Lee, H. K. Baik, B. S. Seong, S. Munetoh, and T. Motooka, Phys. B Condens. Matter **392**, 266 (2007).

[43]T. Duffar, Recent Res. Dev. Cryst. Growth **5**, 61 (2010).

[44]V. A. Oliveira, B. Marie, C. Cayron, M. Marinova, M. G. Tsoutsouva, H. C. Sio, T. A. Lafford, J. Baruchel, G. Audoit, A. Grenier, T. N. Tran Thi, and D. Camel, Acta. Mater. **121**, 24 (2016).

[45]S. Gang, J. Xu, and P. Harrowell, Nat. Mater. **17**, 881 (2018).

[46]F. R. N. Nabarro, Dislocations in Solids (North-Holland Publishing Company, 1979).

[47]F. R. N. Nabarro, Mater. Sci. Eng. **234–236**, 67 (1997).

[48]V. Gerold, Structure of Solids (Cambridge University Press, New York, 1993).

[49]A. Autruffe, V. Stenhjem Hagen, L. Arnberg, and M. Di Sabatino, J. Cryst. Growth **411**, 12 (2015).

[50]T. Zhu and H. J. Gao, Scrip. Mater. **66**, 843 (2012).

[51]Y. F. Shen, L. Lu, M. Dao, and S. Suresh, Scrip. Mater. **55**, 319 (2006).

[52]A. Jerusalem, M. Dao, S. Suresh, and R. Radovitzky, Acta. Mater. **56**, 4647 (2008).

[53]Q. Lu, Z. You, X. Huang, N. Hansen, and L. Lu, Acta. Mater. **127**, 85 (2017).